Efficient Eye Corner and Gaze Detection for Sclera Recognition Under Relaxed Imaging Constraints

S. Alkassar, W. L. Woo, S. S. Dlay and J. A. Chambers

School of Electrical and Electronic Engineering

Newcastle University

Newcastle upon Tyne, UK

Emails: {s.h.m.alkassar, Lok.Woo, Satnam.Dlay, Jonathon.Chambers}@newcastle.ac.uk

Abstract—**Sclera recognition has provoked research interest recently due to the distinctive properties of its blood vessels. However, segmenting noisy sclera areas in eye images under relaxed imaging constraints, such as different gaze directions, capturing on-the-move and at-a-distance, has not been extensively investigated. In our previous work, we proposed a novel method for sclera segmentation under unconstrained image conditions with a drawback being that the eye gaze direction is manually labeled for each image. Therefore, we propose a robust method for automatic eye corner and gaze detection. The proposed method involves two levels of eye corners verification to minimize eye corner point misclassification when noisy eye images are introduced. Moreover, gaze direction estimation is achieved through the pixel properties of the sclera area. Experimental results in on-the-move and at-a-distance contexts with multiple eye gaze directions using the UBIRIS.v2 database show a significant improvement in terms of accuracy and gaze detection rates.**

I. INTRODUCTION

The sclera consists of the white areas of connective tissue and blood vessels within the eye which surround the iris. This part of the eye has a rich pattern of blood vessels which have different orientations and layers [1]. Therefore, the discriminant features extracted from these blood vessels are considered a promising factor for eye recognition under visible-wavelength illumination [2].

There is much research which has investigated sclera recognition in terms of sclera segmentation, feature extraction and matching processes [2]–[8], however, limitations and challenges remain. All recent research in the literature has used only eye images with constrained conditions where the capturing process minimizes noise factors such as close distance capturing with a single eye gaze except in [9]. Our previous work [10] has proposed a sclera recognition system with images which are captured on-the-move and at-a-distance. However, automatic eye gaze detection has not been developed and gaze direction has been manually labeled for each eye image. We therefore, propose the following novel contributions to mitigate the above limitations on a sclera recognition system:

- A novel fusion method for eye corner detection is proposed which is adapted to noise factors;
- An efficient eye gaze detection method which is invariant to eye rotation;
- Operation with sclera images captured on-the-move and at-a-distance is feasible.

The organization of the paper is as follows: in Section II, we propose a new eye gaze detection method. Section III discusses the UBIRIS.v2 database. In Section IV, we introduce our evaluation results and finally we present the conclusions in Section V.

II. PROPOSED EYE GAZE DETECTION

A. Region Of Interest (ROI) Extraction

A cropped eye image normally consists of the iris, pupil, sclera and eyelid skin areas surrounding the eye. To avoid detecting redundant eye corners, we first propose a method to extract the ROI area where eye corners are predicted. We used our method in [8] to extract two diameter arc areas based on skin segmentation to estimate the position and the orientation of the eyelids. As depicted in Fig. 1, the two arc area pixels are defined as

$$\mathbf{Arc} = RGB\left(x_0 + r\cos\theta, y_0 + r\sin\theta\right), \qquad (1)$$

where $\theta \in [-5\pi/12 : 5\pi/12] \cup [-7\pi/12 : 7\pi/12]$ with uniform increment steps of 0.1 degrees and (r, x_0, y_0) are the iris radius and center coordinates calculated by using the
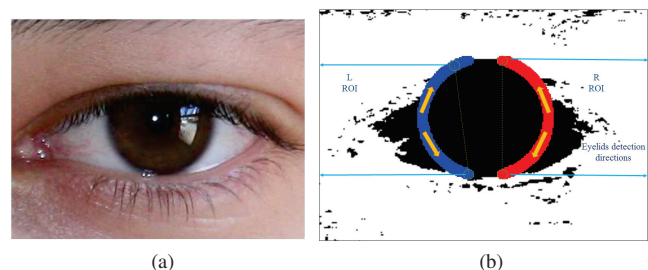

Fig. 1: Eye corner ROI areas detection, (a) an eye image at a distance of 4 meters and (b) the skin segmentation map where R_ROI and L_ROI areas are extracted.
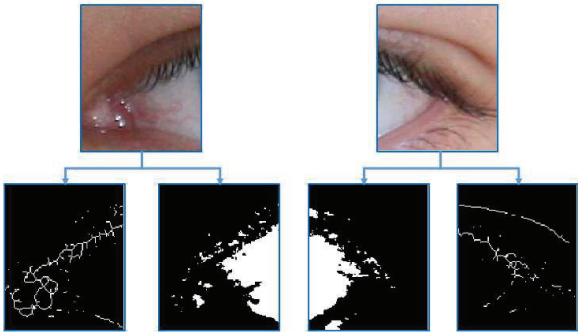
Fig. 2: R_ROI and L_ROI regions each producing two maps for eyelid skeleton border $\mathbf{B}f$ and eyelid skin area $\mathbf{Sk}$.

integro-differential operator [11]. Then, both arcs are divided equally into up and down parts and a circular search for skin pixels on these arcs as depicted in Fig. 1b. The circular search is initiated by taking 100 pixels at a time in the direction $[0 \rightarrow 5\pi/12, 0 \rightarrow -5\pi/12]$ for the right arc and $[\pi \rightarrow 7\pi/12, \pi \rightarrow -7\pi/12]$ for the left arc in order to mitigate incorrect eyelid position. Each portion is checked to determine if these pixels are classified as skin pixels in order to set the y-axis points where R_ROI and L_ROI are cropped.

B. Eyelids Borders Detection and Skin Segmentation

The next step is to extract candidate eye corners. We propose a fusion method to extract corner points by using two maps. The first map represents eyelid border outlines whereas the second map consists of eyelid skin surrounding region pixels. To extract the eyelid border, the saturation level (S) of the HSV color space for R_ROI and L_ROI areas are extracted resulting in $\mathbf{R}s$ and $\mathbf{L}s$ maps. Next, an erosion filter with structure element having a disk shape with size 5×5 is applied on $\mathbf{R}s$ and $\mathbf{L}s$ to eliminate white pixels within the sclera whereas the

sclera has the darkest pixels in the S level. Then, $\mathbf{R}_{er}$ and $\mathbf{L}_{er}$ are subtracted from $\mathbf{R}s$ and $\mathbf{L}s$ to extract the border outlines as

$$\mathbf{B}r = \mathbf{R}s - \mathbf{R}_{er}, \quad \mathbf{B}l = \mathbf{L}s - \mathbf{L}_{er}. \tag{2}$$

Next, binary thresholding is applied on $\mathbf{B}r$ and $\mathbf{B}l$ as

$$\mathbf{B}f = \begin{cases} 1, & \text{if } \mathbf{B}(x,y) > th_i, \\ 0, & \text{otherwise} \end{cases}, \tag{3}$$

where th_i is set empirically to 0.2. Then, binary morphological operations which include removing spur pixels and converting the borders to skeleton form are utilized.

The second map is extracted by complementing the extracted skin segmentation R_ROI and L_ROI maps producing $\mathbf{Sk}r$ and $\mathbf{Sk}l$. This is shown in Fig. 2.

C. Candidate Eye Corner Points Extraction and Gaze Estimation

Next, we extract candidate corner points in $\mathbf{B}f_r, \mathbf{B}f_l, \mathbf{Sk}r$ and $\mathbf{Sk}l$. We use the Harris corner detector [12] to extract corners with a quality level and sensitivity factor equal to 0.3 and 0.01 respectively. To eliminate outlier detected corners, an angle threshold is set with respect to the iris center position from $[-\pi/6 : \pi/6]$ providing 60° of rotation sensitivity.

Next, to estimate the correct corner among all the prospective corner points, we propose calculating the Euclidean distance between all points and returning the point index
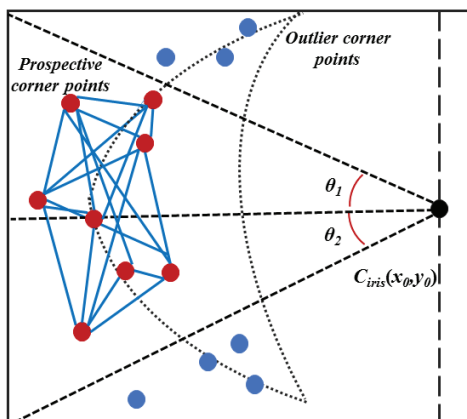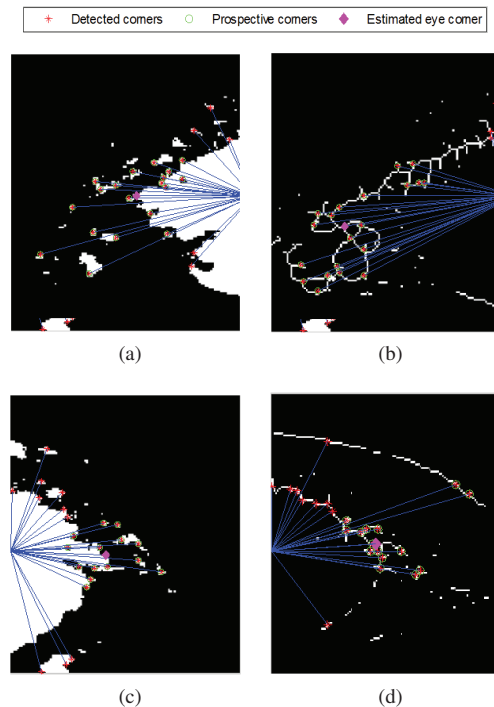

Fig. 3: A diagram represents the proposed angle threshold with respect to the iris center to eliminate outlier corners represented in blue dots and showing a Euclidean distance calculation scheme among prospective corners represented in red dots.

Fig. 4: Eye corner detection for $\mathbf{B}f_r, \mathbf{B}f_l, \mathbf{Sk}r$ and $\mathbf{Sk}l$ for an eye image at a distance of 4 meters, (a) $\mathbf{Sk}l$ mask, (b) $\mathbf{B}f_l$ mask, (c) $\mathbf{Sk}r$ mask and (d) $\mathbf{B}f_r$ mask.
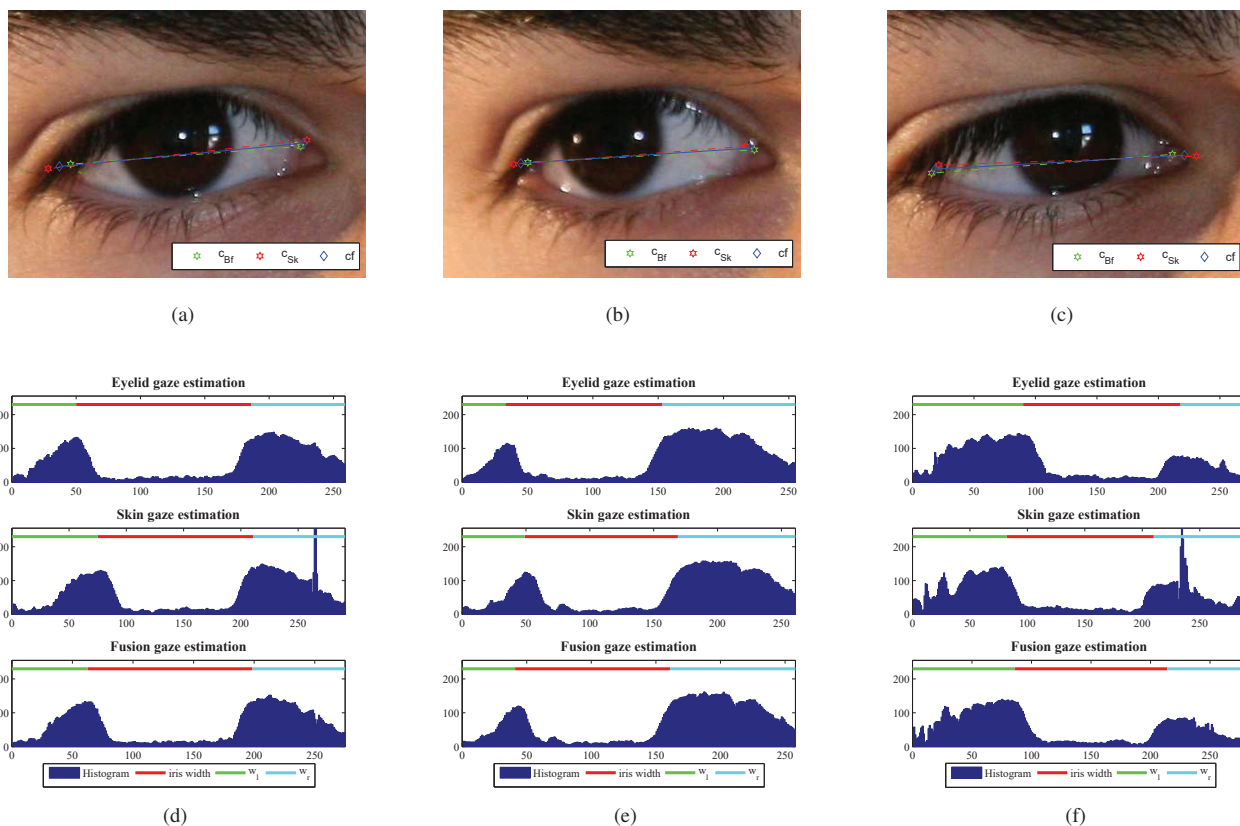
Fig. 5: Examples of the eye gaze detection. (a), (b) and (c) are eye images with F_G, L_G and R_G of the same individual captured at 5 meters; (d), (e) and (f) are the pixel value distribution between detected corners utilizing eyelid border, eyelid skin, and the fusion methods respectively.

which has the lowest distances as depicted in Fig. 3. If the set of prospective corners is $\mathbf{c} = \{\mathbf{c}_1, \mathbf{c}_2, \cdots, \mathbf{c}_n\}$, then the estimated corner point is specified as

$$\mathbf{c}_i = \arg\min_i \left\{ \sum_{j=1}^{n} \|\mathbf{c}_i - \mathbf{c}_j\| \right\}, \qquad (4)$$

where $i \in \{1, \cdots, n\}$ and the symbol $\|.\|$ is the Euclidean distance. As our method for extracting ROI regions ensures that the corner point will be roughly in the middle, then the estimated corner point will has the minimum Euclidean distance with respect to all prospective corner points. Prospective corners and the final corner are shown in Fig. 4.

After detecting the corner point $\mathbf{c}_i$ for eyelid skin segmentation and border maps in both right and left eye sides $(\mathbf{c}_{\mathbf{B}f_r}, \mathbf{c}_{\mathbf{B}f_l}, \mathbf{c}_{\mathbf{Sk}r}, \mathbf{c}_{\mathbf{Sk}l})$, final corner points $(\mathbf{c}f_r, \mathbf{c}f_l)$ are calculated as the points in the middle of straight lines which connect $\mathbf{c}_{\mathbf{B}f_r}$ with $\mathbf{c}_{\mathbf{Sk}r}$ and $\mathbf{c}_{\mathbf{B}f_l}$ with $\mathbf{c}_{\mathbf{Sk}l}$ respectively.

The final step is to estimate the eye gaze direction. The histogram of eye pixels from $\mathbf{c}f_r$ to $\mathbf{c}f_l$ of the eye blue channel in the RGB color space, as this channel introduces more contrast between the iris and the sclera area, is calculated and according to the width of right and left sclera sides, the

decision of eye gaze is defined as

$$Gaze = \begin{cases} \text{R\_G}, & \text{if } (w_l - w_r) \geq th_r \\ \text{L\_G}, & \text{if } (w_r - w_l) \geq th_l \\ \text{F\_G}, & \text{otherwise} \end{cases} \qquad (5)$$

where R_G, L_G, F_G refer to right, left and front gaze respectively, w_r and w_l are the width of right and left sclera areas respectively calculated from the detected corners to iris borders and (th_r, th_l) are the thresholds to determine the eye gaze direction defined as $th_r = 2w_l/5$, $th_l = 2w_r/5$ which control the sensitivity of the eye gaze detection. Examples of an eye gaze detection using eyelid border, eyelid skin and fusion methods and their pixels distribution are shown in Fig. 5.

III. DATASET DESCRIPTION

We used the UBIRIS.v2 database [13] to assess the performance of our proposed method. The database images were captured in unconstrained conditions such as at-a-distance and on-the-move with more realistic noise factors like blurring, rotation and multiple gazes with 300×400 image size. The capturing was performed in two sessions where session 2 was captured by another acquisition device in a different location and luminosity to increase heterogeneity. The number of participating subjects is 261 capturing both eyes resulting

Fig. 6: UBIRIS.v2 eye image examples captured at 6m.

in 522 eye images at distances from 4 to 8 meters. We used 100 images per distance and gaze resulting in 1500 images. We manually marked eye corners for each image in order to create ground-truth comparison samples. Some examples are shown in Fig. 6.

IV. RESULTS AND DISCUSSION

Our simulations were achieved using Matlab (version R2014a) on a PC with Intel core i5 3.0 GHz processor and 8.0 GB RAM. In Fig. 7, ROC curves of the eye corner detection accuracy using the proposed fusion method are plotted with images captured at 5 meters for multiple gazes (F_G, R_G, and L_G). The horizontal axis represents the error pixel threshold where the Euclidean distances are calculated for the detected eye corners with the ground-truth eye corners which manually annotated. It is evident that the fusion method performs best in the front eye gaze direction whereas it achieves lower accuracy for a deviated eye gaze.

To observe the capturing distance effect on our proposed eye corner detection method, we drew ROC curves and boxplots for F_G images captured at distances ranging from 4-8 meters in Fig. 8. We observed that the highest detection rate is when an eye image is captured at 5 meters. This is due to some images at 4 meters distance being cropped removing some parts of the eye corners. However, the detection rate is inversely proportional to the capturing distance. Nevertheless, the median values (horizontal solid lines) and the third quartiles values observed in Fig. 8b, which compares boxplots of the eye corner detection rate, show that the proposed method achieves high performance with images captured at-a-distance
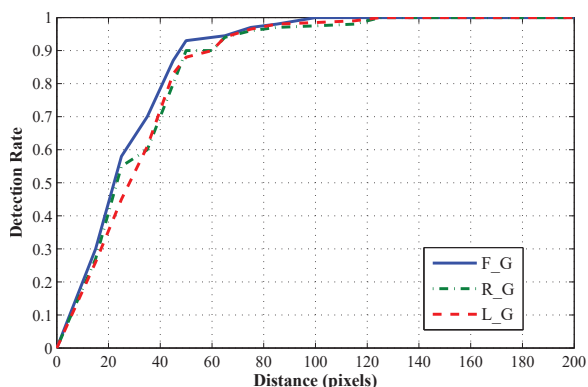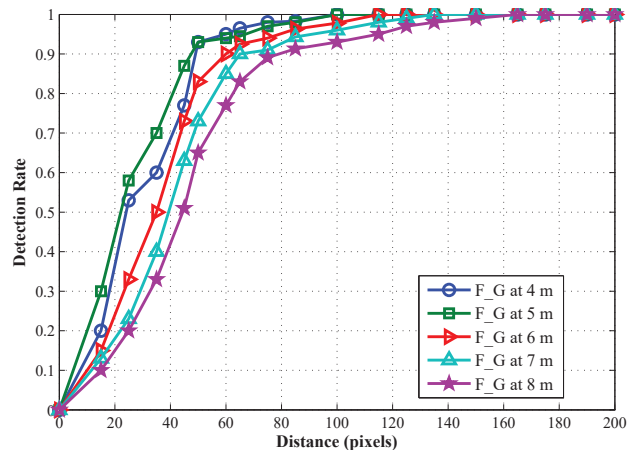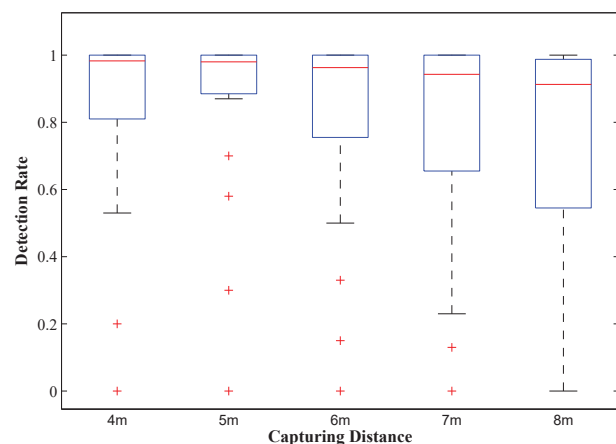

(a)

(b)

Fig. 8: Comparison of detection rates using the proposed fusion method for F_G images captured at distances ranging from 4 to 8 meters. (a) ROC curves and (b) boxplot of the detection rate.

ranging from 4-8 meters. However, the detection rate in the first quartiles values degrades as the distance increases as the quality of images retrograde severely.

In terms of comparing our proposed eye corner detection method with state-of-the-art methods on the UBIRIS.v2 database, we only found one work proposed by Santos and Proenca [14]. However, their method did not involve detecting eye gaze direction. We compared the eye corner detection rate for frontal gaze using 300 images captured at 5 meters. As shown in Fig. 9, our detection method is better than the Santos and Proenca method when the error threshold is less than 40 pixels whereas both methods achieve higher rates after 50 pixels distance threshold.

Finally, we assessed the proposed eye gaze detection methods involving eyelid border detection, eyelid skin detection and fusion detection methods as shown in Table I. As mentioned above, due to the incorrect image cropping for 4 meters captured images which led to removal of eye corners in the

Fig. 7: UBIRIS.v2 ROC curves for the eye corner detection accuracy with multiple gaze directions (F_G, R_G and L_G) using images captured at 5 meters.
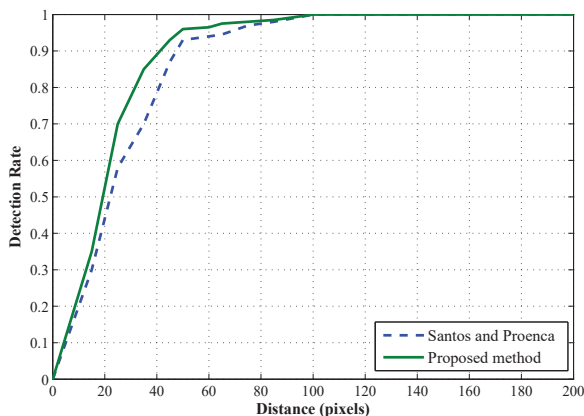
Fig. 9: UBIRIS.v2 ROC curve comparison of proposed eye corner detection with state-of-the-art method due to Santos and Proenca.

UBIRIS.v2, higher gaze detection rate (95%) was achieved with images captured at 5 meters using our proposed gaze detection method. It is also obvious that the larger the image capturing distance, the lower eye corner and gaze detection rates become.

TABLE I: Eye gaze detection rates for the UBIRIS.v2 database images captured at distances range from 4 to 8 meters

(a) Eyelid border method

Gaze Direction	Image Capturing Distance				
	4 m	5 m	6 m	7 m	8 m
F_G	89.6 %	**91.4 %**	85.8 %	81.5 %	76.4 %
R_G	87.4 %	88.7 %	83.2 %	79.3 %	74.6 %
L_G	86.9 %	89.3 %	82.7 %	78.7 %	72.3 %

(b) Eyelid skin method

Gaze Direction	Image Capturing Distance				
	4 m	5 m	6 m	7 m	8 m
F_G	88.3 %	**90.5 %**	83.6 %	79.9 %	72.6 %
R_G	86.6 %	89.2 %	80.1 %	76.6 %	71.6 %
L_G	87.4 %	88.1 %	81.2 %	77.1 %	70.2 %

(c) Fusion method

Gaze Direction	Image Capturing Distance				
	4 m	5 m	6 m	7 m	8 m
F_G	93.3 %	**95.2 %**	92.7 %	89.3 %	83.1 %
R_G	90.1 %	94.2 %	92.5 %	85.7 %	81.7 %
L_G	91.0 %	91.9 %	93.1 %	84.4 %	80.4 %

V. CONCLUSION

In this paper, novel eye corner and gaze detection methods have been proposed to overcome limitations in using relaxed imaging constraints in sclera recognition. Eye corner detection has been achieved through an adaptive fusion method depending on the eyelid borders and eyelid skin properties. In addition, an efficient method for eye gaze detection has been suggested to overcome the change in rotation and distance of sclera areas when an eye image is captured. The results using the UBIRIS.v2 database showed that our proposed eye corner and gaze detection methods have high detection rates for different distances and gazes thus introducing more robustness. This paper has not however suggested a new method for iris segmentation under unconstrained imaging which our method depends on and remains as future work.

REFERENCES

[1] C. Oyster, *The Human Eye: Structure and Function*. Sinauer Associates, 2006. [Online]. Available: https://books.google.co.uk/books?id=n9yoJQAACAAJ

[2] Z. Zhou, E. Y. Du, N. L. Thomas, and E. J. Delp, "A new human identification method: sclera recognition," *IEEE Trans. Syst., Man, Cybern. A*, vol. 42, no. 3, pp. 571–583, 2012.

[3] R. Derakhshani, A. Ross, and S. Crihalmeanu, "A new biometric modality based on conjunctival vasculature," *Proc. of Artificial Neural Networks in Engineering (ANNIE)*, pp. 1–8, 2006.

[4] R. Derakhshani and A. Ross, "A texture-based neural network classifier for biometric identification using ocular surface vasculature," in *Int. Joint Conf. on Neural Networks. IJCNN*. IEEE, 2007, pp. 2982–2987.

[5] S. Crihalmeanu and R. Derakhshani, "Enhancement and registration schemes for matching conjunctival vasculature," in *Proc. of the 3rd IAPR/IEEE Int. Conf. on Biometrics (ICB)*, 2009, pp. 1240–1249.

[6] K. Oh and K.-A. Toh, "Extracting sclera features for cancelable identity verification," in *Int. Conf. on Biometrics (ICB), 2012 5th IAPR*, 2012, pp. 245–250.

[7] Y. Lin, E. Y. Du, Z. Zhou, and N. L. Thomas, "An efficient parallel approach for sclera vein recognition," *IEEE Trans. Inf. Forensics Security*, vol. 9, no. 2, pp. 147–157, 2014.

[8] S. Alkassar, W. L. Woo, S. S. Dlay, and J. A. Chambers, "Robust sclera recognition system with novel sclera segmentation and validation techniques," *IEEE Trans. Syst., Man, Cybern., Syst.*, vol. PP, no. 99, pp. 1–13, 2016.

[9] S. Alkassar, W. L. Woo, S. S. Dlay, and J. A. Chambers, "Enhanced segmentation and complex-sclera features for human recognition with unconstrained visible-wavelength imaging," in *2016 Int. Conf. on Biometrics (ICB)*, June 2016, pp. 1–8.

[10] S. Alkassar, W. L. Woo, S. S. Dlay, and J. A. Chambers, "A novel method for sclera recognition with images captured on-the-move and at-a-distance," in *2016 4th Int. Conf. on Biometrics and Forensics (IWBF)*, March 2016, pp. 1–6.

[11] J. Daugman, "How iris recognition works," *IEEE Trans. Circuits Syst. Video Technol.*, vol. 14, no. 1, pp. 21–30, 2004.

[12] C. Harris and M. Stephens, "A combined corner and edge detector." in *Alvey Vision Conf.*, vol. 15, Manchester, UK, 1988, p. 50.

[13] H. Proena, S. Filipe, R. Santos, J. Oliveira, and L. Alexandre, "The ubiris. v2: A database of visible wavelength images captured on-themove and at-a-distance," *IEEE Trans. Pattern Anal. Mach. Intell.*, vol. 32, no. 8, pp. 1529–1535, 2010.

[14] G. Santos and H. Proença, "A robust eye-corner detection method for real-world data," in *Biometrics (IJCB), 2011 Int. Joint Conf. on*. IEEE, 2011, pp. 1–7.